Biomagnetic Monitoring vs. CFD Modeling: A Real Case Study of Near-Source Depositions of Traffic-Related Particulate Matter along a Motorway

Sarah Letaïef, Pierre Camps, Thierry Poidras, Patrick Nicol, Delphine Bosch, Romane Pradeau

Biomagnetic Monitoring vs. CFD Modeling: A REAL Case Study of Near-Source Depositions of Traffic-Related Particulate Matter along a Motorway

Sarah Letaïef [1,*], Pierre Camps [1], Thierry Poidras [1], Patrick Nicol [1], Delphine Bosch [1] and Romane Pradeau [1,2]

[1] Géosciences Montpellier, University of Montpellier, CNRS, 34090 Montpellier, France; pierre.camps@umontpellier.fr (P.C.); thierry.poidras@gm.univ-montp2.fr (T.P.); patrick.nicol@gm.univ-montp2.fr (P.N.); delphine.bosch@gm.univ-montp2.fr (D.B.); romane.pradeau@sfr.fr (R.P.)

[2] Géoressources and Environnement, Bordeaux INP and Univ. Bordeaux Montaigne, ENSEGID, 1 allée F. Daguin, 33607, Pessac cedex, France

* Correspondence: sarah.letaief@umontpellier.fr; Tel.: +33-627-818-611

Received: 27 September 2020; Accepted: 20 November 2020; Published: date

Abstract: A test site located along a 12-lane motorway east of Montpellier, France, is used to evaluate the potential of biomagnetic monitoring on traffic-related particulate matter (PM) to parametrize a computational fluid dynamics (CFD) simulation of the local airflow. Two configurations were established on the site with three vegetated flat-top earth berms of a basic design, and a fourth one was located windward to the traffic roofed with a 4-m-high precast concrete wall. As a first step, PM deposition simultaneously on plant leaves, on low-cost passive artificial filters, and on soils was estimated from proxies supplied by magnetic and X-ray fluorescence measurements on both sides of the motorway. These latter revealed that traffic-related pollutants are present on soils samples highlighted with a clear fingerprint of combustion residues, and wears of breaks, vehicles, and highway equipment. Maximum PM accumulations were detected in the lee of the berm–wall combination, while no significant deposition was observed on both sides of the flat-top earth berms. These results are in line with measurements from PM μ-sensors operated by the regional state-approved air quality agency. Finally, we compared the experimental measurements with the outcomes of a computational fluid dynamics (CFD) modeling based on the Reynolds-Averaged Navier–Stokes (RANS) equations that consider the traffic-induced momentum and turbulence. The CFD modeling matches the experimental results by predicting a recirculated flow in the near wake of the berm–wall combination that enhances the PM concentration, whereas the flat-top berm geometry does not alter the pollutants' transport and indeed contributes to their atmospheric dispersion.

Keywords: traffic-related PM; motorway; biomonitoring; environmental magnetism; X-ray fluorescence; CFD; openFoam

1. Introduction

Nowadays, one of the growing concerns in our society is the quality of the air we breathe, which is most likely because the proportion of city dwellers in the world drastically increased from 29.6% to 55.3% between 1950 and 2018 [1], respectively. Indeed, urbanization comes with a rise in the activities damaging air quality in a close environment to the living places. Broadly, the transports, the energy production used for heating or industrial activity, as well as the knock-on effect of civil engineering and building are widely identified as major threats to the surrounding air. In addition, urbanization is often combined with a suburban sprawl, making people more car-dependent. As expected, the main source of pollution in urban and peri-urban areas would be unequivocal road traffic [2,3], for which the combustion of fossil fuels, vehicle and road equipment wears, and

resuspension processes contribute to a large part of urban particulate matter (PM) emissions including ultrafine particles (UFP) (<30 nm). It is now well established that PM is a carrier of reactive metals into the respiratory system, causing a variety of short and long-term adverse health effects because metals are not biodegradable [4]. The sizes of UFP are so small that they foster health issues, since they can pass through the lung wall to the bloodstream, affecting the cardiovascular system and possibly reach organs such as the brain [4–6]. The societal issue is important. The latest models reported by the European Environment Agency [7] assess the number of premature deaths by exposure to fine particles at 412,000 for European countries in 2016, which represents more than 4 millions of years of life lost, knowing that these numbers may have been underestimated [8]. Citizens are now well informed of this danger and increasingly try legal action as a way to ensure that the cities become a safer place to live. At the level of European actions, six countries including France are in litigation since May 2018 and referred to the European Union Court of Justice for non-compliance with the limit values of nitrogen dioxide and PM concentrations [9]. It is important to bear in mind that the European regulatory warning levels are more lenient standards than the World Health Organization air quality guidelines. Another worrying factor for the urban residents concerns the regulatory measurement protocols. Yielding concentration in $\mu g/m^3$, they do not promote the monitoring of ultrafine particles being too light to be detected.

In this context, the present work comes with a citizen mobilization in an eastern Montpellier city of 3500 inhabitants, Saint-Aunès, France, which is a riparian city of the A9 motorway. The mobilization began in response to a program intending to expand this motorway from a dual 3-lane motorway to a dual 6-lane motorway that raised concerns about the noise and the air quality. In response to the mobilization, an experimental site composed of four vegetated earth berms bordering the carriageways had been built by the motorway company (Figure 1). Earth berms are structures mainly built for noise abatement strategy [10]. Their impact on air pollution lessening is seldom studied [11] in contrast to that of alternative structures such as solid or vegetative noise barriers, e.g., [12–17]. The population expectations on the air quality issue coincide with effective ways and means of evaluating the efficiency of this local noise barrier setup. Remarkable and most likely unique, the experimental site was instrumented in July 2017 with in particular eight fixed stations equipped with e-PM™ µ-sensors. The system has been designed and operated for a 10-year monitoring by the regional state-approved air quality agency. In this project, we were mandated to assess the effectiveness of shrubs and trees present on the berms for monitoring, and subsequently for mitigating, the particulate matter released from traffic.

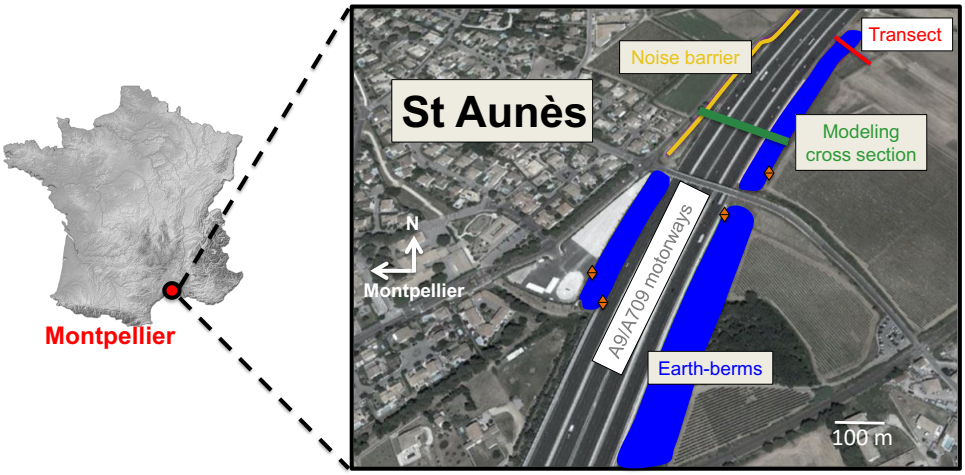

Figure 1. Map of the study area locating in blue the three flat-top berms; the one roofed with a precast noise barrier is in yellow, and the soil samples transect is in red. Orange arrows indicate the location of the regional air agency PM microsensors, and the green line illustrates the location of the modeling cross-section. Image from Google Earth V7.3.3.7721. digital Globe 10 July 2018.

The link between vegetation and air pollution has been the subject of substantial research over the past decades whether on monitoring [18] or on mitigation issues [19,20]. As yet, the mitigation by urban green is not topical, because the plants installed in 2017 on the berms are still too small to significantly influence the spatial apportionment of pollutants. Thus, we can only stay focused on the monitoring component without addressing the impact of vegetation installed on the berms on air quality. Once the pollutants deposition on plant leaves is time-integrated by accumulation, the assessment of pollution uptake by plants with analytical measurements may provide a low-cost near-source specific record supplementing the direct measurements with PM sensors. Among the different techniques of plant tissues analyses, environmental magnetism is now commonly implemented in biomonitoring approach because it yields proxies of relative concentration in trace metal on a large measuring interval with a very good resolution [21]. This cheap and rapid–approach allows us to measure amounts of samples making achievable high-resolution mappings of near-source deposition. The underlying assumption is that empirical relationships exist between the trace elements deposition on plant leaves and the plant leaves' magnetic properties [22]. When applied to traffic-related sources, this link is often observed [23,24] because vehicles present concomitant emissions of trace elements and iron, either coated on the surface of spherule of carbon cores in vehicle exhaust [4] or in close association in wear products. Iron is found in the form of iron oxides such as magnetite, hematite, or maghemite, presenting a magnetic behavior [25] easily caught on accumulating surfaces. Strong correlations found between Pb, Fe, and magnetic parameters [22] may also suggest that trace elements can be directly incorporated into crystalline structure of the iron oxides.

In first part, we will report on the magnetic characterization of plant leaves, soil samples, and artificial filters together with X-ray fluorescence (XRF) measurements in order to map the near-source PM deposition along the motorway. Then, the spatial PM distribution will be compared to results of a pseudo-3D micro-scale atmospheric CFD model considering both the motorway environment (berms, curbs, and slope of the carriageways) and the fleet-induced turbulence and momentum. The key issue is whether and how precisely can the magnetic biomonitoring constrain a state-of-the-art CFD modeling of traffic pollutant dispersion. Finally, the results will be discussed and compared to the trend observed from the PM μ-sensors operated by the regional agency of air quality.

2. Materials and Methods

2.1. Study Area

The ASF motorway company, in agreement with the city of Montpellier and the French state, has carried out between 2014 and 2017 a major project to double the A9 motorway over 25 km with the objective to streamline traffic by separating the 265,000 vehicles which circulate on the daily average around Montpellier on two six-lane routes. In fact, the huge construction site has brought out two separated routes. One is used by motorists who wish to stay on the highway, and the other is used as a peripheral for services to Montpellier city. These two roads meet at the northeast end at the village of Saint-Aunès that is bordered by a 12-lane motorway. To prevent excessive noise impacts at residences and educational facilities, two configurations (Figure 1) were established: three flat-top earth berms with a vegetated roof and one roofed by a precast noise barrier. To carry out this study, we obtained from the motorway company the topographic maps of the site indicating the location of the various structures, the traffic data over 4 months, and an agreement to access the motorway domain for sampling directly on the berms.

2.2. Sampling

A prerequisite for magnetic mapping traffic-related PM deposition on accumulating surfaces is to check first the relationships between the trace element content and the magnetic parameters in a close location to pollutant emission. To this end, a first sampling was composed of 6 endemic species found on the earth berms, namely, *Cupressus sempervirens*, *Ciste monspeliensis*, *Quercus ilex*, *Salvia rosemarinus*, *Coronilla valentina*, and *Cercis siliquastrum* on one hand, and on the other hand soil

samples taken at the rooting depth of these same plants. Plant leaves were harvested by cutting them by the stem with a clean chisel and directly dropped into a plastic bag without being touched with a hand to avoid contamination during collection. Soil samplings were realized with clean plastic tools. In the laboratory, due to the complications of XRF measurements when water is present, plant samples were dried in an oven at 80 °C during 24 h and then placed in a desiccator during cooling down to the room temperature and finally crushed to powder with a hand agate mortar and pestle. Soil samples were firstly sieved under 2 mm grain size and then dried in the same way as the plants and ground to finally be sieved again under 0.3 mm grain size. Each sample of plants and soils was reduced to dried powder were divided in 3 and 6 aliquots in order to average the results, respectively, and placed into XRF sample cups SC-4131-0 closed on top with a polypropylene film. We used polyester fiber stuffing to fully complete the filling of the cups to prevent sample movements. Dried sample masses were estimated with an analytical microbalance (Sartorius ENTRIS 224i-1S, Sartorius, Goettingen, Germany) by means of a double weighting operation to subtract the mass of the sample holders. This design allows us to measure X-ray fluorescence and magnetic characteristics on a same preparation if care is taken to subtract the empty sample-holder signal.

A second campaign of sampling was realized in accordance with our main objective to map by means of magnetic measurements the deposition of traffic-derived PM along the motorway. To this end, we used three different types of accumulating surfaces located in the motorway near environment. The first type was natural plant leaves. Particles passive trapping and retention on plant leaves is influenced by several factors as the plant type deciduous or evergreen, the leaf surface area, the micro-surface roughness, the presence of hairiness or leaf veins, and the thickness of their waxy cuticle at the leaf surface [26–28]. Assessing the atmospheric pollutants uptake on plant leaves is further hampered by plant capacity to absorb trace metals from soil via their root system and translocation to leaves [29]. To sum up, analytical data from plant tissues are difficult to apprehend and decipher unless a single plant species is harvested close to and around the point source emission being investigated in order to reduce as much as possible adverse inputs from environmental variabilities or from undesired sources. The deciduous species *Cercis siliquastrum* was selected because it is abundant on the earth berms and nearby, it presents a large surface leaf area, and it is not known to have capacity for trace elements translocation from soils to leaves. A total of 25 *Cercis siliquastrum* trees were sampled in a single day on 2 July 2019, which represents a good spatial coverage of the study area. Their heights vary from 0.50 m on vegetated earth berms to a few meters for a tree close to the noise barrier side or the trees outside the motorway domain. About 15 leaves by tree, representing a total surface in the range of 150 to 680 cm^2, were collected by always keeping in mind to favor leaves of similar sizes located at the tree canopy. This way, we ensure the homogeneity and the representativeness of the sampling. Since magnetic measurements are not sensitive to the water content, fresh leaves were directly packed into 8 cm^3 plastic cubes sample holders in order to reduce handling and thus minimize spurious changes of the signal, either by contaminations or cleaning. After the magnetic treatment and measurement, leaf surface areas were measured with a CI-202 laser area meter (cid Bio-Science™, Camas, WA, USA). This procedure aims to reduce the laboratory operations to keep unaltered the dust deposition on plant tissues prior to the analyses. The second type of accumulating surface used for mapping was quantitative paper filters of 2–3 μm particle retention. To prevent mechanical weathering by insects or water saturation by rainfall that could have the effect of reducing their filtering surface, they have been inserted inside the mounting design proposed by Cao et al. [30]. The assembly is composed of a plastic electrical box of a circular section of 50.6 cm^2 in which filters were placed between two layers of washed natural wool to absorb excess moisture. The whole is closed by a piece of 1 mm mesh canvas allowing only the entry of fine particles. A total of 30 artificial filters have been positioned on both sides of the motorway from 25 May to 25 August 2019. For some stations, filters were put as a duplicate to leaves, whereas for others, only artificial filters were analyzed. In the laboratory, the paper filters were placed also into 8 cm^3 plastic cubes sample holders for magnetic measurements. Finally, we also took 31 soil samples on a transect perpendicular to the highway on the northernmost flat-top earth berm (red line on Figure 1). Samples were taken on a surface of 30 cm by 30 cm on the first 2 to 3 cm depth after

cleaning the area of vegetation and coarser materials such as gravels or pebbles. They were prepared for the analyses in the same way as those harvested in the first sampling and were divided each into three aliquots.

2.3. Elemental Analysis

Chemical elemental analyses were performed with the Niton XL3t-900 Goldd X-ray fluorescence portable analyzer (Thermo Scientific®, Waltham, MA, USA) on ex situ samples reduced to powder after drying. Before specimen analyses, sample holders with their specific design were empty measured to discard if necessary the ones that may have a negative impact on measurements due to a strong signal. The interpretation of XRF spectra was processed in two steps. We have certified the presence of an element from a qualitative visual inspection of spectrum before to calculate its concentration with the NITON Data Transfer software provided by Thermo Electron Corporation™, Waltham, MA, USA. Results are obtained in μg/g (ppm).

2.4. Magnetic Treatments and Measurements

An Isothermal Remanent Magnetization (IRM_{1T}) was first imparted at 1 Tesla to all the empty sample holders, with the impulse magnetizer ASC Model IM-10-30 from ASC Scientific, and then measured with a 2G-SQUID cryogenic magnetometer. Subsequently, these operations were repeated after loading fresh plant leaves, paper filters, or soil and plant powders into their respective sample holders. Magnetic moments expressed in Am^2 were corrected by subtracting the magnetic moment of an empty sample holder, which was then normalized by the leaf area or by the sample mass, yielding the IRM_{1T} intensity of the samples in Ampère (A) or in Am^2/kg, respectively. Given the possible presence of impurity contents in the plastic molding, the sample holders could potentially carry more or less magnetization. This two-step protocol becomes required since we are unable to magnetize the samples without magnetizing the sample holders at the same time. Such a two-step protocol is applicable in the present case because the magnetic moment of the sample holders (on the order of a few 10^{-9} Am^2) is between 1 and 3 orders of magnitude smaller than that of the samples. Furthermore, IRM intensity is a practical proxy of bulk magnetic contaminant concentration which may be in turn subject to instabilities due to the magnetic viscous effect of variable relaxation times [31] if sufficiently small magnetic nanoparticles are present as often observed in magnetic biomonitoring survey [32]. As it is routinely done in our laboratory, samples were placed in a zero-field following the IRM acquisition until the magnetization is stable enough. We checked the stability of the 1T-magnetization imparted to the empty and to the filled sample holder and found a very small magnetic viscous effect characterized by a relaxation time lower than 2 and 10 min, respectively (see Figure A1). Then, the duration of stay in zero-field following the IRM acquisition and prior to the measurements was set to a minimum of 15 min for all samples.

2.5. Numerical Simulation of Transport of Particles Emitted from Local Traffic

We have implemented a computational fluid dynamic (CFD) approach to simulate the micrometeorological characteristics that directly affect the dispersion of pollutants in the atmosphere. The purpose was to analyze the three-dimensional dispersion of fine particles emitted by the traffic at the measuring sites and in the surroundings. To this end, we used the openFoam (open Field Operation and Manipulation. Available online: http://www.openfoam.com (accessed on 9th September 2020)) open source toolbox that is freely available.

For the particles transport, we followed a conventional Eulerian approach that uses the advection–diffusion equation e.g., [33–35] treating the concentration of particulate matter (PM) as a passive scalar quantity C advected by an incompressible wind fluid $\mathbf{u}$. The general formulation of the temporal change of C combines the advection and the diffusion equations with a source term Sc describing the creation of C and a sink term due to particle settling as following:

$$\frac{\partial C}{\partial t} = -\nabla \cdot (C\mathbf{u}) + \nabla \cdot (\Gamma_D \nabla C) + S_c - U_s \nabla C \cdot \mathbf{n_z} \quad (1)$$

where C (μg/m³) is the transported PM concentration, t is the time in seconds, **u** is a stationary velocity field (m/s) computed from a microscale meteorological model, Γ_D is the effective diffusion coefficient (m²/s) of C in air, S_c (μg/m³) is the source term of C, U_s is the particle settling speed (m/s), and $\mathbf{n_z}$ is a vertical unit vector introduced here for homogeneity. In Equation (1), several terms require further explanations. First, the effective diffusion (Γ_D) combines the laminar (Γ_L) and the turbulent (Γ_T) diffusion components [33], $\Gamma_D = \Gamma_L + \Gamma_T$. The laminar mass diffusivity component Γ_L is assessed by means of the Stokes–Einstein equation:

$$\Gamma_L = \frac{\zeta T C_c}{3\pi\mu d_p} \quad (2)$$

where ζ is the Boltzmann's constant (1.38 × 10⁻²³ kg m² K⁻¹ s⁻²), T is the absolute temperature (K), d_p is the aerodynamic diameter of particles (m), and μ is the dynamic viscosity of the air (18 × 10⁻⁶ kg m⁻¹ s⁻¹). C_c is the dimensionless slip correction factor given by

$$C_c = 1 + \frac{\lambda}{d_p}\left[2.34 + 1.05\, e^{-0.39 d_p/\lambda}\right] \quad (3)$$

where λ is the mean free path (set here to 0.066 μm). The turbulent mass diffusivity component Γ_T is given by

$$\Gamma_T = \frac{\nu_\tau}{Sc_\tau} \quad (4)$$

where ν_τ (m²/s) is the eddy viscosity, which is calculated during the resolving of the velocity field **u,** and Sc_τ is the turbulence Schmidt number, a dimensionless constant describing the relative diffusion of momentum and mass, arbitrarily set to 0.7 in the present study. Second, the particles settling speed U_s is derived from $U_s = C_c \tau_p g$, where g is the gravitational constant (m·s⁻²) and τ_p is the particle relaxation time (s), which is equal to $\rho_p d_p^2/18\mu$ with ρ_p as the particle density (kg·m⁻³).

The fundamental assumptions for such modeling are that (i) the transported species within the flow does not affect the air flow, (ii) which is assumed to be incompressible and isothermal. Thereby, Equation (2) is easily resolved when both the source term S_c for a class of particles with known aerodynamic diameter and a velocity field **u** are prescribed.

2.5.1. Assessment of the Emission Source Term (S_c)

Emissions of particulate matter induced by traffic have been steadily decreasing over the past decades thanks to technological innovations in engine design, new fuel composition, and high efficiency particulate filters at the exhaust pipe up to developments in techniques for collecting microparticles emitted by disc braking systems. The second observation we made is that the in-use motor vehicle fleet can be very heterogeneous. For example, in Europe, the motor vehicle fleet is getting older year-on-year, reaching 11 years on average in 2017 [36]. Therefore, we found it beyond the bounds of possibility to accurately estimate particulate traffic emissions directly from the traffic data. Instead, we have opted to use as the best estimate the latest measurements made in tunnels that have the advantage of characterizing real-world traffic at a given time, including particles from the resuspension of dust, from combustion products, and from vehicle and road structure wear. The survey carried out in 2015 in the Shing Mun Tunnel (Hong Kong) and Fort McHenry (Baltimore, MA, USA) [37] gives us an average emission rate for the PM2.5 of 0.025 g.veh⁻¹.km⁻¹ for a mixed light/heavy-duty traffic. We will remain focused on PM2.5 because the direct measurement of PM10 was not carried out in this study and the only data we found relate to ancient measurement campaigns carried out in 2006 in Hatfield Tunnel, London, UK [38] and in 1999 in Tuscarora Mountain tunnel, PA, USA [39], which may not be representative of the current fleet emissions.

2.5.2. Assessment of the Velocity Field **u**

The experimental measurement of particle deposition on surfaces being by nature cumulative over a few months, the statistical steady Reynolds-Averaged Navier–Stokes (RANS) turbulence

model was chosen to solve the fluid flow. The Reynolds decomposition adopted in steady RANS is addressed in approximating the instantaneous movement of the fluid in order to solve only the equations of the time-averaging field, which somewhere favors the duration of the observation compared to the turbulence timescale. Steady RANS is an open set of equations needing further approximations for closure commonly achieved by means of the Boussinesq hypothesis relying on the concept of the eddy viscosity (ν_τ) (see [40] for a review). We chose the standard k-ε first-order closure model that was proposed by Jones and Launder [41] for high Reynolds-number flows and recently validated for atmospheric boundary layer and particles dispersion [35,42]. In this closure model, the eddy viscosity is given by:

$$\nu_\tau = \rho C_\mu \frac{k^2}{\varepsilon} \quad (5)$$

where the turbulence kinetic energy (k) and its dissipation rate (ε) are estimated from their transport equation, ρ is the air density, and C_μ is a model constant fixed to 0.09.

In the literature on near-road air pollution impact, the velocity field is generally only resolved from local atmospheric conditions. With very few exceptions [43,44], the modeling of pollutant dispersion and deposition does not include velocity momentum and turbulence generated mechanically by the traffic whether for verisimilar urban environments [45] or for different roadside barrier configurations [11,46,47] or for true road networks [48]. In the present case, it would be a rough approximation to exclude the traffic input on the mean velocity field and on turbulence for two reasons. The earth berms under consideration have a height comparable to that of the heavy goods vehicles circulating on the motorway, and the traffic density for the 12 lanes combined is rather significant with an average of 264,550 vehicles per day calculated over 4 months, from May to August 2019. One way to account for the traffic is to introduce in the atmospheric model source terms in a finite volume over the carriageways. Therefore, the velocity field was set in two steps.

In a first step, the challenge was to determine the average vehicle-induced momentum (VIM) corresponding to the velocity in the wake and the average vehicle turbulence (VIT) that comprises the turbulent kinetic energy (k) and its turbulent dissipation rate (ε) that could be representative as much as possible of the real average traffic. To meet this challenge, we constructed a zero-wind and flat-terrain precursor CFD model from the average traffic density calculated from May to August 2019 for a single carriageway for both A9 and A709 motorway (2 × 3 lanes). Four vehicle templates including one heavy goods vehicle, one motorhome, one family car, and one sport car available under the common creative license were used to mimic the fleet (Digital designs for physical objects. Available online: https://www.thingiverse.com (accessed on June 29th 2020)). The distance between consecutive vehicles driving on the same lane was calculated from the traffic density assuming that all vehicles move at a constant speed of 25 m·s^{-1} that corresponds to the speed limit. A total of 17 and 21 "stand still" vehicles were placed in the correct proportion between light-duty and heavy goods vehicles on the 3 lanes along a 620 m stretch of the A9 and the A709 motorways, respectively. The length corresponds to the minimum length, allowing us to simulate an average traffic as close as possible to that calculated from the data. To simulate a permanent and continuous traffic, we applied periodic conditions at the beginning and at the end of the modeled carriageway section. All the other computational domain boundaries have been set to moving wall condition with a constant speed of 25 m·s^{-1}. The CFD domain extent is 620 m long × 48 m wide × 28 m high, presenting thus a cross-section large enough to avoid erroneous estimate due to blockage effect. Two control volumes (cross-sectional area of 5 × 10 m) centered on the A9 and A709 carriageways, respectively, were used to estimate the vehicle-induced average momentum and the vehicle-induced average turbulence.

In a second step, the wind velocity field in the atmospheric boundary layer affected by volume sources representative of the bi-directional 12 lanes traffic, by the road structures such as the 0.9 m high and 0.2 m wide concrete curbs separating the carriageways, and by the topography of the earth berms was resolved. A pseudo-3D CFD simulation was designed by extruding along the third dimension a 2D topographic profile transverse to the carriageways obtained from the motorway company. Doing thus, the berms are continuous throughout the lateral domain extension, limiting the simulations to scenarios with wind perpendicular to the carriageways. Furthermore, this

limitation was forced by the periodic boundary conditions applied at the front and back domain boundaries to simulate continuous traffic. Such refinement nullifies the possibility for real-3D CFD simulations with slanted wind direction relative to the motorway structures.

We followed the best practice guidelines [49] to determine the size of the computational domain. The vertical extension of the domain was fixed at a minimum of 22H (176 m) to prevent an artificial acceleration of the flow over the top of the noise barrier located at 1H (5 m or 8 m when measured relative to the ground west to the motorway or to the carriage way, respectively). In that respect, the corresponding blockage in the flow direction—defined as the ratio between the noise barrier area to the free-stream cross section of the computational domain—is kept below 5% whether the wind comes from one side or from the other. The lateral extension of the domain was arbitrarily set to 120 m. This choice did not appear sensitive in our simulations because we only considered a pseudo-3D geometry for the topography and because periodic conditions have to be set up on the lateral boundaries of the computational domain. The extension of the domain in the flow direction was set up with a geographic positioning at 8H and 35H for the inflow and outflow boundaries, respectively, relative to the location of the closest earth berm of height equal to 1H. The distance of 35H appeared to be sufficient in the different tests we carried out to allow for flow redevelopment behind the berm, avoiding thus the possibility for the fluid to re-enter through the outflow boundary.

The computational domain was meshed in two steps. A coarse mesh with hexahedral cells of 8 m side length was created with the openFoam utility blockMesh and then refined in close proximity of the ground and the motorway structures with the openFoam utility snappyHexMesh. The minimum thickness of the cells was fixed to 0.03 m close to the ground level with a maximum aspect ratio of 1.2. This ensured a good overall grid resolution with at least three cells between the ground level and the monitoring site locations (Figure 2). At the end of the refinement, the total number of cells is 1349 million. Four cell zones of a theoretical volume of 6000 m^3 each (cross-section 5 × 10 m, Figure A2) were defined over each 3-lane carriageway to enable inputs of the vehicle-induced momentum, the vehicle-induced turbulence, and the particle emissions source terms into the model.

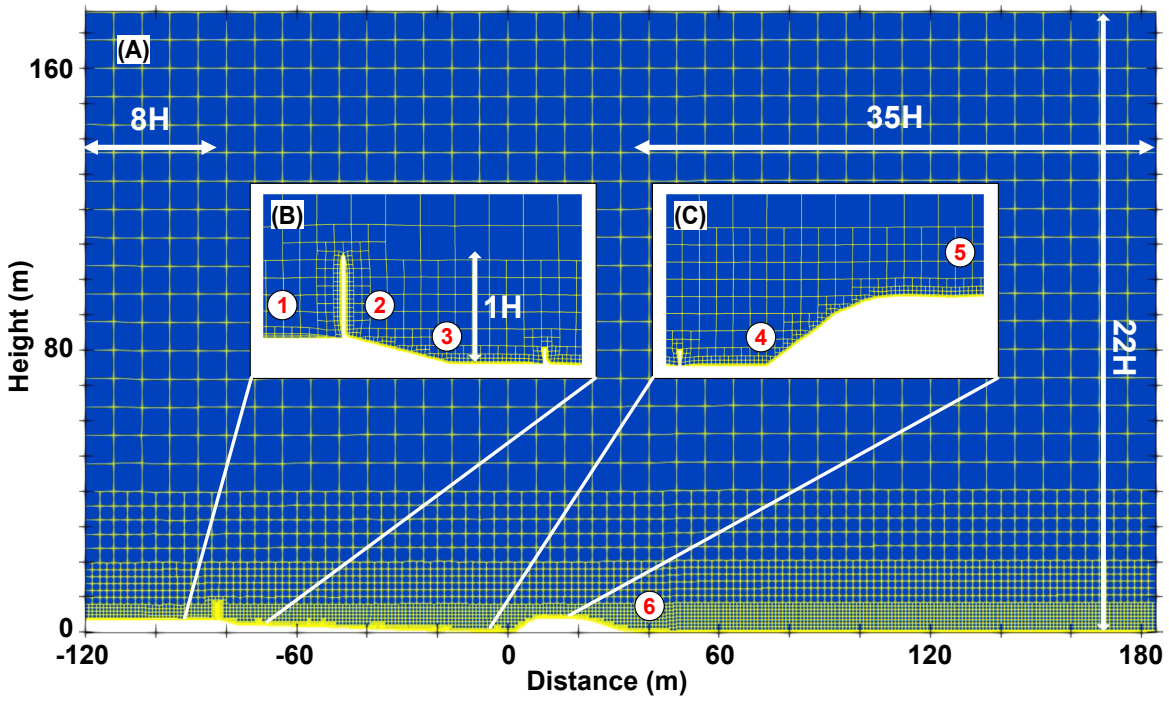

Figure 2. Overview of the meshing from the front of the domain (**A**), with a zoom on the precast noise barrier atop of a berm here located upwind to the source (**B**) and a zoom on the flat-top earth-berm located downwind to the source (**C**). Numbers in red show the locations of the vertical profiles at which the PM2.5 concentrations are monitored.

Boundary conditions were set accounting Richards and Norris [50] recommendations for the k-ε turbulence model applied to a neutral atmospheric boundary layer. In this context, constant properties in directions tangential to the ground were assumed. For the velocity, they call for a wind velocity profile with the elevation of the log-law type, a driving shear stress at the upper boundary, and a near wall velocity matching up approximately the inlet profile at the ground boundary. Thus, the velocity inlet profile was prescribed by means of:

$$U = \frac{U^*}{\kappa} ln\left(\frac{z - z_g + z_0}{z_0}\right) \quad (6)$$

where U^* is the friction velocity, κ is the von Karman's constant, z is the vertical coordinate (m), z_0 is the surface roughness (m), and z_g is the ground altitude if is not equal to zero. We fixed z_0 to 0.1 m to characterize the open country with occasional obstacles present on the both sides of the motorway. Dirichlet conditions are applied at the upper and at the lower boundaries equal to the velocity in the inlet at the upper height in order to ensure the driving shear stress and equal to zero (no-slip) at the ground level to enable the viscosity-affected region to be resolved, respectively. In a neutral atmospheric boundary layer, the turbulence kinetic energy and its dissipation rate have an analytical solution in RANS simulation that was used for inlet boundary conditions:

$$k = \frac{(U^*)^2}{\sqrt{C_\mu}} \quad (7)$$

$$\varepsilon = \frac{(U^*)^3}{\kappa(z - z_g + z_0)}. \quad (8)$$

We acknowledge that a constant value with height for the turbulence kinetic energy is debatable, since it is observed neither in field measurement nor in wind tunnel experiment [40,51]. However, the recommendations in the literature do not clearly prohibit the use of these relationships, which are selected here since they correspond to the analytical solutions of the k-ε closure model. A zero gradient in wind direction was prescribed for k and ε as the upper boundary condition by means of a free slip condition. The standard model k-ε can only be used in highly turbulent flows, which is no longer found in regions close to the walls. Then, the use of wall laws is a solution to consider the presence of viscous effects to simulate the inner region between the wall and the turbulence fully developed region. We utilized the standard rough wall functions for k and ε available in the openFoam libraries. For all the variables, the Neumann zero gradient condition was applied at the outlet boundary except for the pressure for which a Dirichlet fixed value set to zero was applied. As stated previously, periodic boundary conditions were applied at the front and at the back boundaries to consider a continuous traffic.

The wind velocity field was resolved by means of the pressure-correction method SIMPLE-C [52] with a very stable numerical approximation based on first-order discretization schemes for the first thousand steps, which was followed by a very accurate numerical approximation based on second-order discretization schemes ensuring 4 orders of residue falls to indicate the convergence. This technique helps to start a solution in the presence of the thin wall noise barrier and the concrete curbs that could represent strong discontinuities in the topography, which may give rise to solver stability problems. The stability of the calculation is further secured by means of under-relaxation factors chosen as high as possible while ensuring no oscillations in the flow solution.

3. Results

3.1. Magnetic Mapping of Near-Source Depositions of Traffic-Related Particulate Matter

Prior to the magnetic mapping, the pair-wise relationship between magnetic properties and chemical contents of deposition on accumulating surfaces such as plant leaves or soils was first checked by means of a bivariate scatter plot. In Figure 3, we plot the IRM intensity imparted with a 1-T magnetic field against the total concentration of 13 main elements, namely Mo, Pb, As, Zn, Cu, Ni, Co, Fe, Mn, Cr, V, Sb, and Cd from measurements made on the same sample of plant or soils. At the first order, the form of the relationship is clearly linear. It is characterized by a concomitant increase of the two parameters that makes sense from a physical point of view if our working

hypothesis is correct; the more the iron and associated metal content is high, the more the laboratory-imparted magnetization is strong. The strength of this relationship is evaluated by means of the Pearson's product-moment correlation coefficient, which is estimated to 0.80 with a *p*-value of 8.4×10^{-9} calculated for the alternative hypothesis that the true correlation is not equal to zero; the pair-wise positive linear relationship appears to be strong enough to validate the working hypothesis. The Spearman's rank correlation coefficient was also calculated because it is more appropriate in the present case, since the two variables are not normally distributed. Equal to 0.84 with a *p*-value of 1.3×10^{-7} and close to the Pearson coefficient value, it confirms a strong linear positive relationship. However, this conclusion is moderated by considering only the various plant species by excluding the soil samples from the analysis (Figure 3B). The Pearson's and the Spearman's correlation coefficients are reduced to 0.69 (with a *p*-value of 5.06×10^{-4}) and to 0.74 (with a *p*-value of 1.97×10^{-4}), respectively.

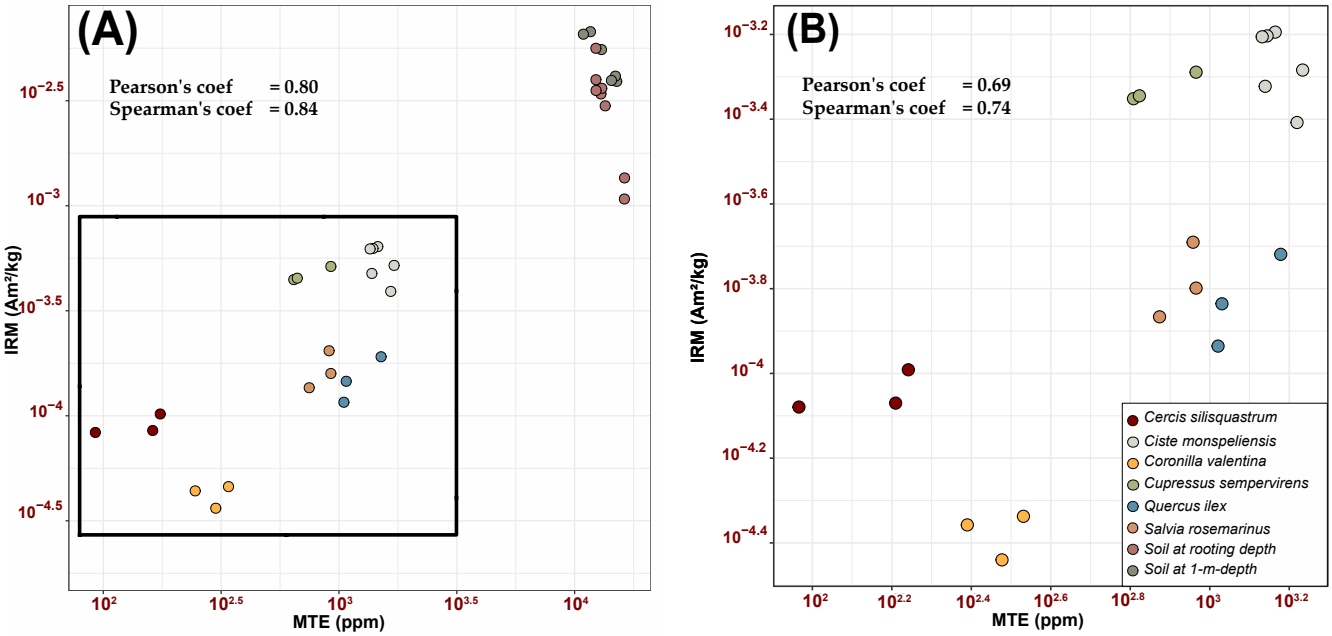

Figure 3. Relationships between Isothermal Remanent Magnetization (IRM_{1T}) and concentration in main trace elements (MTE; Mo, Pb, As, Zn, Cu, Ni, Fe, Mn, Cr, V, Sb) for soils and plant leaves (**A**), and only for plant leaves (**B**) harvested on earth-berm.

Next, we tried to verify the traffic origin of the PM deposition by identifying the vehicle-related tailpipe, non-tailpipe, and natural emissions from trace elements associations. To this end, a principal component analysis (PCA) was performed with the FactoMine R package tools [53] on selected chemical elements characteristic of traffic emissions such as Te, Cs, Ba, Sb, Ni, Sn, Zr, Sc, Sr, Zn, Pb, Cr, U, V, Mo, Hg, As, Mn, Se, Fe, and Cu. Unfortunately, we have been able to perform such analysis solely on soil samples because many targeted chemical elements are present in soil but there are not enough concentrated on plant leaves. Principal component analysis on trace elements derived from XRF data reveals three clusters of relatedness (Figure 4). The first two components account for 42.5% of the total variance in the dataset. Cluster 1 is mainly composed of Sc, Sr, Zn, and Pb and is negatively correlated with cluster 3, which represents associations between Cr, V, As, Mn, Se, Fe and Cu elements. On the other hand, cluster 2 demonstrates associations between Te, Cs, Ba, Sb, and Zr chemical elements. The traffic origin seems clear. Elements in cluster 1 are often associated with fuel and additive residues [54–57], elements in cluster 2 are mostly linked to vehicle wear on the roadway [55,57,58], and finally, elements in cluster 3 may be linked to the vehicle and highway equipment wear [56,59,60]. This interpretation is further validated with the analysis of the ratio of Cu:Sb. This ratio is considered as highly discriminating between brake wear particles characterized by values lower than 10 [61], and natural particles characterized by much larger values, which are greater by at

least one order of magnitude. All the soil samples from the earth berm yielded a Cu:Sb ratio lower than 10, with a mean value of 6.2 ± 2 supporting the hypothesis of a significant traffic input on soil surface of the earth berms.

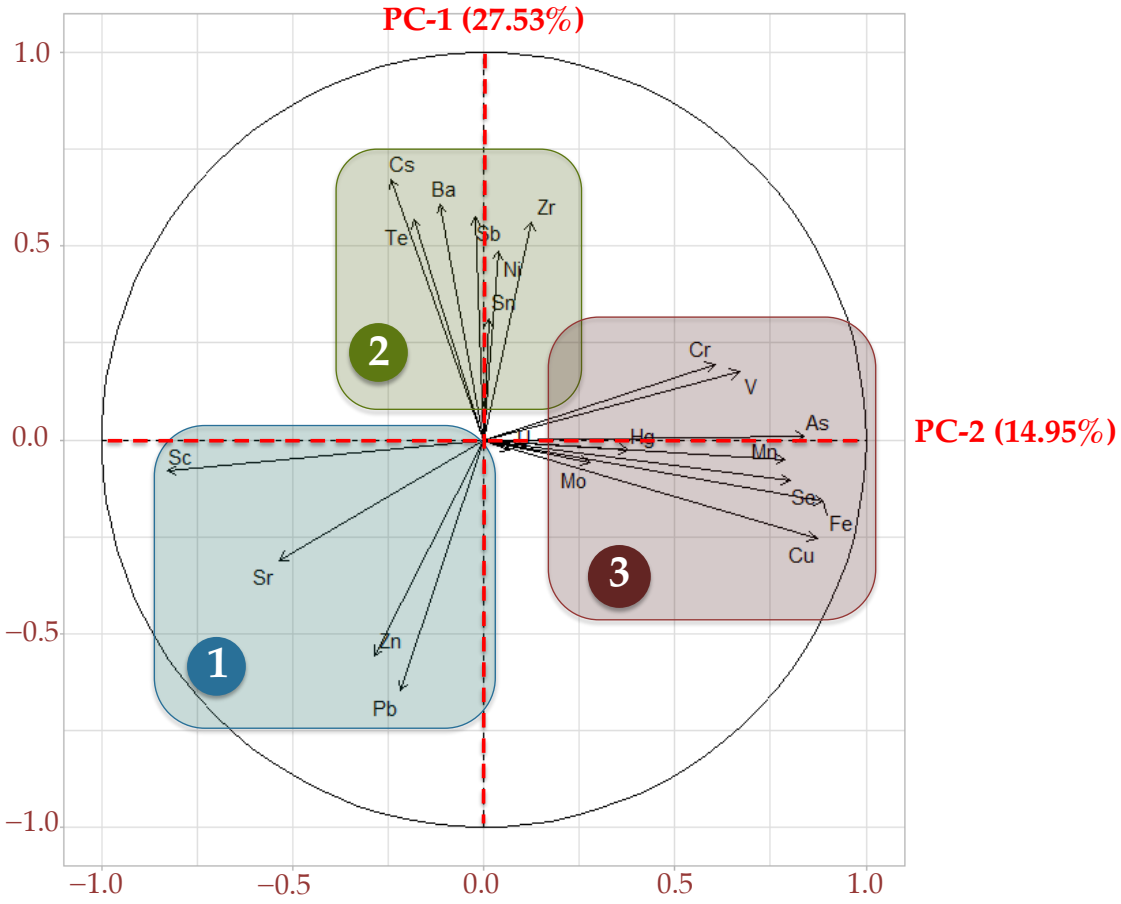

Figure 4. Principal component analysis revealing principal trace metallic sources.

Hence, the magnetic mapping of depositions of trace elements related to the local traffic seems to be soundly based in the present survey. Nevertheless, we believe that it is important to subtract from the total signal the signal from the deposition of PM related to the regional background level. This latter is assessed with reference samples taken from remote areas assumed to be non-impacted by emissions from similar sources that the ones surveyed. The choice of their location is important in magnetic monitoring and should be wisely selected to allow meaningful comparisons. To this end, we chose reference stations for plants and filters located in a forest and in a village north of Montpellier, respectively. For soil samples, we directly drilled the top of the earth berm with an auger to take references samples at a depth of about 1 m, assuming that no pollutant transfer occurs from the soil surface. To depict the near-source deposition, we will use the relative change (*RC*) parameter given by:

$$RC = \frac{IRM_{(1T,traffic)} - IRM_{(1T,reference)}}{IRM_{(1T,reference)}}. \quad (9)$$

As such, *RC* is a unitless number that pays attention to the amount at which the traffic-related "magnetic" PM estimated form $IRM_{(1T,\ traffic)}$ superimpose to the background PM estimated from $IRM_{(1T,\ reference)}$. Results are presented on Figure 5. A similar trend between artificial passive filters and *Cercis siliquastrum* leaf samples is observed. Roughly, higher PM concentrations are highlighted in the near wake of the earth berms located upwind of the traffic where relative change values are 4 to 10 times higher than those from the reference stations, while no significant PM deposition seems to

occur to the flat-top earth berms downwind to the traffic. This observation seems to be counterintuitive. More predictably, PM concentrations are higher on the traffic side rather than the opposite side, highlighting a positive screening effect of the noise barrier structure on air quality.

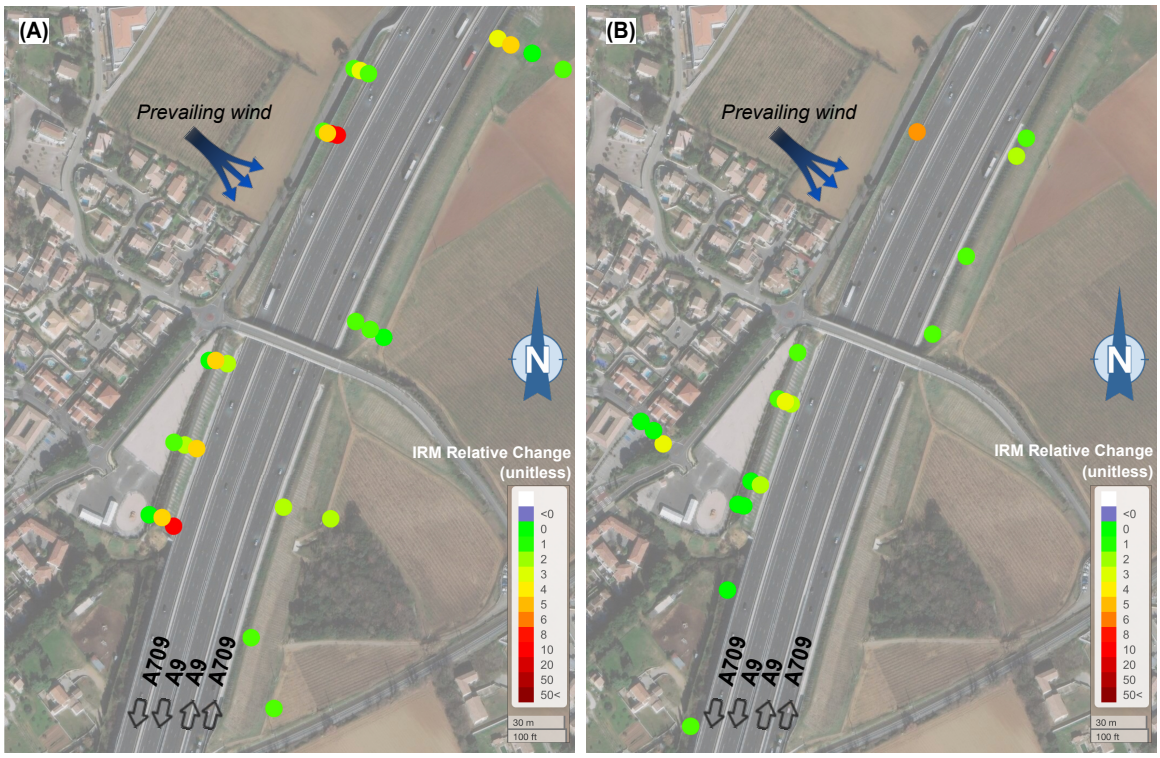

Figure 5. Maps of traffic-derived particulate matter (PM) measured by Isothermal Remanent Magnetization (IRM) relative change (RC) on: (**A**) artificial filters and (**B**) *Cercis Siliquastrum* leave samples. Image from Google Earth V7.3.3.7721 digital Globe 10 July 2018.

The signal measured on soils taken along the transect in the lee of the carriageways (see localization on Figure 1) is more difficult to interpret (Figure 6). The relative change with the reference sample is weak with values close to zero, even showing slightly negative values. In addition, we do not observe a gradient in the magnetic signal further away from the source. This may be exactly opposite to what we might have expected for the deposition of local traffic-related PM, since the concentration of particles should decrease as a function of distance from the source due to dispersion and deposition processes.

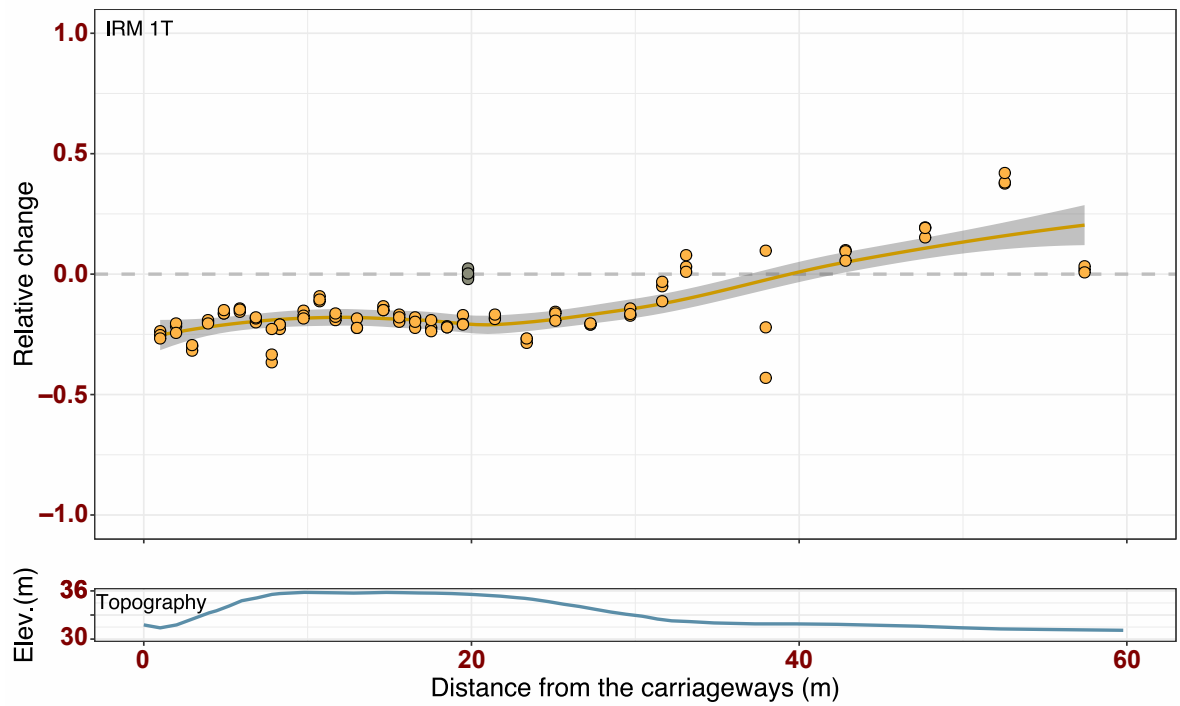

Figure 6. Relative changes from surface soil samples (yellow closed circles) along the transect shown on Figure 1. RC are calculated with a reference sample (gray circles) taken at 1-m depth with an auger from the top of the berm.

3.2. PM Dispersion Modeling Results

The openFoam test cases were uploaded to the Zenodo open-access repository [62] and are available under the Common Creative license to reproduce the results obtained in the present study.

Equation (1) was resolved with the scalarTranportFoam solver included in the open source openFoam platform tools after having made some slight modifications to the source code in order to consider the turbulent diffusivity. This modification is required, since for PM in general [33] and for PM2.5 in particular, the effective diffusivity (Γ_D) is mainly controlled by the turbulent diffusivity (Γ_T) rather than the laminar (Γ_L) diffusivity. In the present case, Γ_T computed from the model outcome with Equation (4) is within the range 10^{-3} to 10^{1} m^2s^{-1}, which compares with 1.007×10^{-11} m^2s^{-1} for Γ_L calculated with Equation (2) applied to PM2.5. The scalarTransportFoam solver also does not consider the gravitational settling term. However, no change is required in this sense because the settling speed (Us) being equal to 2.12×10^{-4} m s^{-1} for PM2.5, the gravitational settling term can be neglected without adversely affecting the results. The emission source term *Sc* is entered in Equation (1) as a volumetric source assuming that the vehicle pollutants are homogeneously thinned down and mixed in a volume over the carriageways by the fleet-induced turbulence and momentum. Here, Sc is distributed over four rectangular cuboids of a cross-sectional of 5 × 10 m area each and a length corresponding to the full width of the domain (see Figure A2 for illustration). These volumetric sources are centered on each 3-lane carriageway. We applied PM2.5 emission values equal to 0.35 and 0.42 $\mu g.m^{-3}$ s^{-1} for A9 and A709 motorways, respectively, which were calculated from the traffic data (Table 1) and an overall PM2.5 emission rate of 0.025 g $veh^{-1}.km^{-1}$ found in the bibliography for a current mixed light/heavy-duty traffic [37].

Table 1. Mean daily traffic density used to calculate fleet momentum and turbulence. LD and HD are daily numbers of light duty and heavy duty vehicles with their respective proportions used in the model (LD:HD). Distance corresponds to the distance between two consecutives vehicles. Note that only the numbers in bold characters are derived from traffic data (see text for explanation) in the north–south direction. We assumed that these values are the same for traffic in the opposite direction.

U, k, and ε are the average velocity deficit, average turbulent kinetic energy and average turbulent dissipation rate, respectively, derived from the modeling.

Lane	LD	HD	Total	LD:HD	Distance (m)	U (ms^{-1})	k (m^2s^{-2})	ε (m^2s^{-3})
A9 Motorway								
right	9441	9441	18,882	3:2	114			
middle	25,176	3147	28,323	7:1	76			
left	12,742	0	12,742	4:0	170			
			59,947			7.3	2.1	1.3
A709 Motorway								
right	21,696	3616	25,312	6:1	85			
middle	32,009	0	32,009	9:0	68			
left	16,004	0	16,004	5:0	135			
			73,325			6.5	1.7	0.9

The stationary field u in Equation (1) was calculated in two steps. By means of a precursor zero-wind model, the mean fleet-induced turbulence and momentum were calculated from an average traffic configuration constructed from 4-month-averaged daily data provided by the motorway company. In the absence of precise information on traffic volume by lane, we have arbitrarily distributed the proportion of vehicle on each lane with the only constraint preventing heavy goods vehicles from using the leftmost lane reserved to the light-duty vehicles. Furthermore, care has been taken to keep the ratio between light- and heavy-duty vehicles for the 3-lane carriageways close to the data. From this vehicle density, we calculated a distance between two consecutive vehicles by considering that all vehicles travel at the maximum authorized speed of 90 km/h. Therefore, our model has a perfectly realistic but obviously not unique configuration. The model parameters and the metrics of turbulence and momentum derived from the zero-wind model are given in Table 1 and illustrated in Figure 7. These parameters are calculated over a volume of a cross-sectional area of 5 × 10 m along the full length of the domain fixed from the vehicle density design in this precursor model at 620 m. They are subsequently used in a second step as volumetric turbulence and momentum source terms in the atmospheric wind modeling over the same volume as the one used for pollutant emissions. Five different inlet profiles were considered in the atmospheric wind modeling through different friction velocity U* values in Equation (6): four in the prevailing wind direction and one in the opposite direction. We calculated U* in order to obtain reference velocities of 5, 7, 10, and 12 ms^{-1} at a height of 8.5 m corresponding to the top of the precast noise wall atop of the earth berm for the prevailing wind direction cases, and 7 ms^{-1} at a height of 4 m corresponding to the top of the flat-top earth berm for the opposite wind direction case. Traffic-related PM2.5 concentrations are monitored along six vertical profiles that are located on Figure 2 and are illustrated in Figure 8.

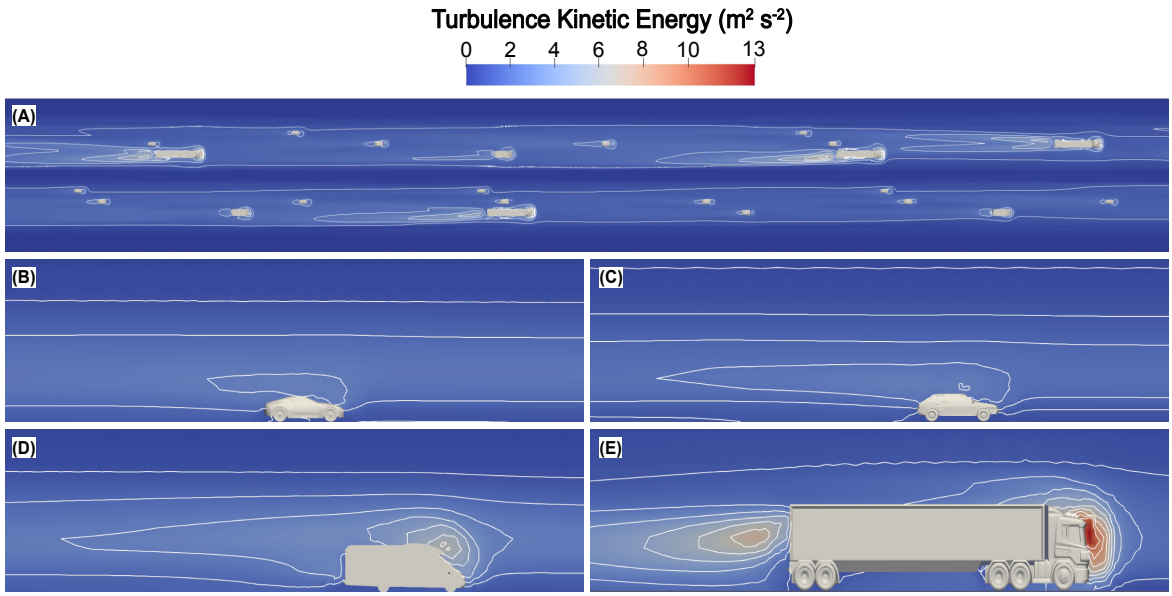

Figure 7. Turbulence kinetic energy obtained in a zero-wind flat terrain model in which all the fleet moves with a speed of 25 m/s. (**A**) Downward zoomed view from the top of the domain, (**B**–**E**) zoomed view from the front of the domain of the four vehicle types used in the model, which are are (**B**) sports car, (**C**) family car, (**D**) motorhome, and (**E**) heavy goods.

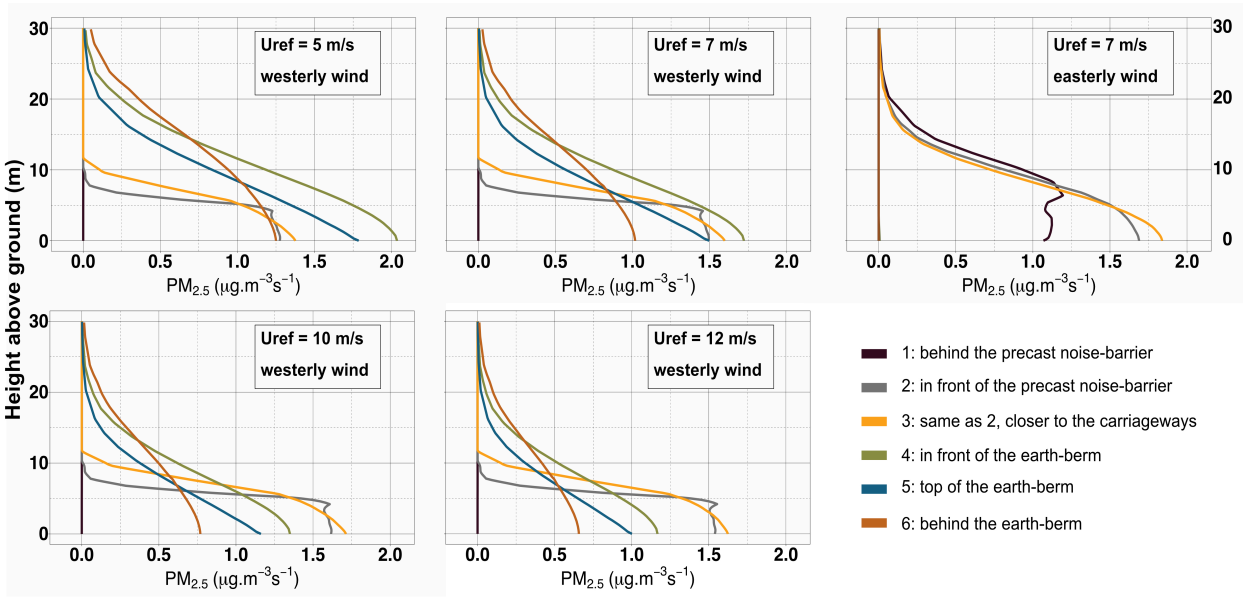

Figure 8. $PM_{2.5}$ concentration calculated along six vertical profiles localized on both sides of the berm roofed with a precast noise barrier and the flat-top earth berm (see Figure 2) with reference velocities of 5, 7, 10, and 12 m/s in the prevailing wind direction and 7 m/s in the opposite wind direction.

3.3. E-PM µ-Sensors Recording

We used the analytical data published in a public report of $PM_{2.5}$ concentrations carried out by the regional air agency from 9 August to 24 September 2019 (Figure 9) that were obtained by means of e-PM™ µ-sensors. These non-certified and not precisely calibrated micro-sensors only provide relative information with respect to each other. According to the engineers in charge of these measurements, the measured value cannot be directly interpreted. Consequently, we calculated from the daily means the relative change with Equation (9) between measurements done in front of (motorway side) and behind (opposite side) the earth berms, assuming this later as the reference measurement. Close to zero, within the limits of the precision of these devices, it would seem that the

flat-top earth berm downwind to the traffic does not play a role in retaining the pollutants, whether in terms of blockage or in terms of dispersion. These observations are in line with the CFD modeling results.

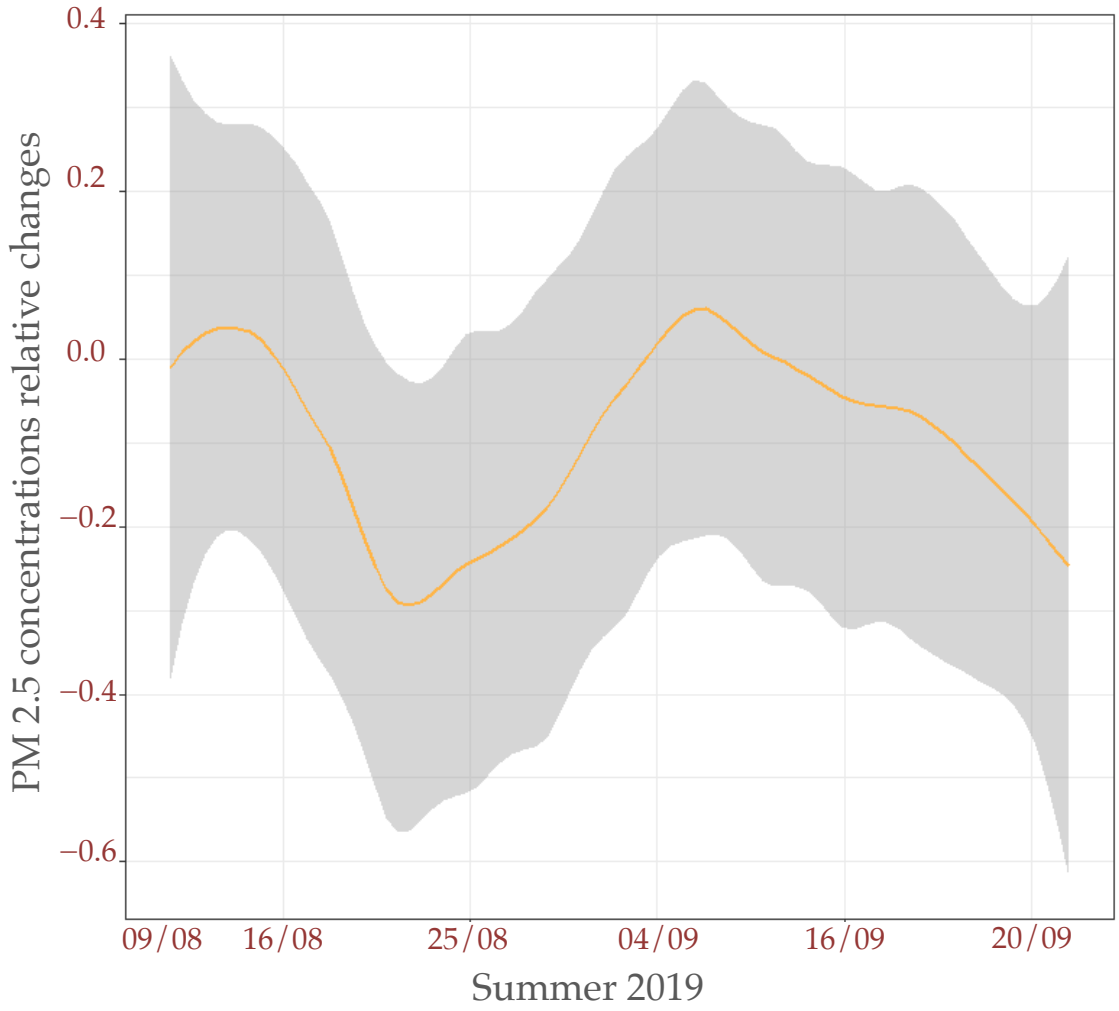

Figure 9. Relative changes calculated from e-PM μ-sensors located in front (traffic side) and behind (opposite side) the flat-top earth berm. We used Equation (9) with as the reference measure the record behind the earth berm.

4. Discussion

4.1. Quality of the Magnetic Measurements

As it has been widely discussed in numerous studies [21], our survey confirms that imparting in the laboratory and then measuring an isothermal remanent magnetization on accumulative surfaces can be a useful and reliable proxy for air quality. This inference is based on the observation of a similar pattern of near-traffic pollutant deposition yielded from measurements on both artificial filters and plant leaves corroborating the outcomes of a CFD numerical modeling. This result validates a posteriori several intrinsic hypotheses of the magnetic approach. For instance, it may indicate that the measurements on the *Cercis Siliquastrum* leaves are not biased by the phenomenon of translocation of elements from the soil to the leaves. It could also validate that the rain has no impact on featuring the spatial general trend of PM deposition. Whether wet accumulation of atmospheric particles or on the contrary leaching phenomenon, we hypothesize that a bias introduced by rain, if any, should be cancelled out by the calculation of the relative change with respect to a reference measurement assuming a constant influence of the rain at the local scale. This hypothesis needs to be further tested in the future by simulating, for example, artificial leaching on

some plants. Obviously, this question does appear to deserve a study in its own right. Of course, this remark remains valid concerning all the parameters that could cause variance in the magnetic response not linked to the surveyed source of pollutants. We think in particular on the nature and on the domain-like behavior of the magnetic oxides, assumed with no certainty to be identical over the entire study area including the reference sample. Two results require a specific comment.

The first concerns the weak strength in the pair-wise correlation observed in Figure 3B between the magnetization intensity and the concentration in main trace elements. We believe that the unexplained variance is induced by an unsuitable sample preparation chosen to be well suited for the XRF experiments. By drying and reducing samples to powder, it is quite likely that a variable and unknown quantity of pollutants might be lost during handling. Alternative protocols such as leaching and filtering the surface settling should be tested when XRF and magnetic measurements have to be carried out on the same samples. Another track to explore to address the weakness of this correlation is the normalization of magnetic measurements by the sample masses. Doing this, we included the parameter of the thickness of the leaves, which can be variable from one leaf to another and which plays no obvious role in the catchment efficiency by a leaf's surfaces. When only a magnetic measurement has to be made, we recommend reducing the handling by working on fresh samples and by normalizing the measurements per unit of area, which is similar to what we did to build the mapping of PM deposition illustrated in Figure 5. From a physical point of view, measuring fresh leaf samples does not have any impact on the magnetic measurements, since water presents a diamagnetic behavior, which is not detected as soon as a small amount of ferromagnetic (lato sensu) particles is included in dust composition.

The second concerns the meaning of the measurements carried out on the soil samples taken at the earth berm surface along the transect perpendicular to the traffic lanes. In one hand, the surface soil samples have clearly a traffic signature highlighted with PCA analysis (Figure 4) and a Cu:Sb ratio lower than 10. On the other hand, the magnetic signal does not provide evidence for a surface enrichment with traffic-related PM in regard to the sample reference (Figure 6), regardless of the distance from the motorway along the earth-berm transect. Without further analyses, we can tentatively imagine that our preferred scenario is the following. We know from the motorway company that the clay materials used to build the earth berm were collected during the construction along the former motorway and possibly they could have been taken from an old retention pond for storing the runoff waters on the original carriageways. Since the former motorway was built over fifty years ago, we can assume that these clays have been exposed to a significant pollution prior their present use as earth berm. Thus, the measured chemical signal would be an inherited signal. The reworking of the clays during the berm construction would explain the homogeneity of the signal. Considering that this earth berm was built in 2017, this implies that the two years during which the earth-berm surface was exposed to the present traffic are not long enough to accumulate traffic products in a sufficient quantity to be detected by magnetic and geochemical proxies. We note that this scenario is compatible with the results of the CFD modeling showing a relatively low concentration of pollutants at the earth-berm surface as well as with the μ-sensor data. A second scenario that may perhaps be considered involves a migration of pollutants from the surface to the subsoil driven by percolating water. Regardless of the possible explanation, soil samples from earth berms do not appear to be good candidates for pollutants monitoring.

4.2. Determination of the Sources of the Traffic-Related PM from Elemental Analysis

Our attempt to precisely determine the sources of trace elements from elemental XRF analysis is questionable. First of all, this approach is limited because it requires sufficient concentrations in trace elements that we have only found in soils, thereby excluding plant leaves from this analysis. In the specific case of soil samples collected on earth berms, a pollution inheritance problem such as the one we have highlighted in this study may shadow the signal being queried. Next, it should also be recognized that the determination of the sources by means of associations between trace elements as yielded from the PCA analysis (Figure 4) is not straightforward and can be tricky to decipher. The main reason is that the correlation between elements can vary widely according to distinctive

regional characteristics of the traffic and the period under consideration. The type of road and asphalt pavement, the speed limit, the ratio between light and heavy duty vehicles, the fuel type, and also the local climatic conditions are the main factors impacting the emission type and the relative contributions from exhaust and non-exhaust emissions [61]. For instance, the United States of America first forbade the leaded gasoline in 1975, followed by Europe in 2000. Even if Indian and Chinese fuel quality standards generally mimic European ones, regional features may be observed, since cities and regions in China can develop and implement their own fuel quality standards, while India currently has two fuel quality standards [63]. So, it would not be correct to compare the elemental composition of traffic emission with those from other non-European countries. In our approach, the main issue remains probably the era because most of the papers we quoted are older than ten to fifteen years, which makes the comparisons pretty complex. Indeed, a survey only based on comparison with results found in the bibliography is less suitable than a study that would have first characterized the signature of the current local traffic. Since the nature and the origin of pollutant are everchanging, a relevant approach is to jointly perform elemental or isotopic analyses in tunnel e.g., [55,64] under similar driving conditions. Unfortunately, we were not able to carry out such comparison in the present study. Finally, despite all these caveats, we believe that the widely used Cu:Sb ratio remains efficient to detect the signature of the braking system wear [61]. These two elements are easily detected by XRF measurements, and the threshold values characteristic of a natural and a traffic signal are significantly different.

4.3. Biomagnetic Monitoring vs. CFD Simulations

The mapping of traffic-related PM depositions illustrated in Figure 5 is characterized by an asymmetry between the two sides of the traffic lanes, which seems to be mainly driven, in addition to the wind direction, by the noise barrier design configuration.

Surprisingly, we did not observe a significant airborne accumulation on filters and plant leaves collected on the leeward side of the carriageways from the flat-top earth berms. The signal measured on soils, although more complex to analyze, seems in line with this observation. The same remark applies to the PM concentrations provided with the e-PM™ μ-sensors, as illustrated in Figure 9. The slope of the earth berm calculated for noise deflection while limiting sound reflection on its source side appears also in the CFD modeling very effective in creating an upward deflection of the incoming air flow promoting the dispersion of fine particles in the atmosphere. Then, the low PM concentration in the near wake of the flat-top earth berm is explained by the absence of down-flow or recirculating flow behind the berm (Figure 8). Therefore, for the case where the source is downwind of the flat-top earth berm, i.e., wind in the opposite direction of the prevailing wind, the local traffic does not contribute to the PM concentration on the berm, as shown in Figure 8. The influence of the flat-top earth berm in the pollutant concentration at greater distance away from the motorway could not be assessed here, since this study was designed to stay focused on the near-source deposition.

Just as startling, the concentration of PM appears to be more important in the near wake of the wall noise barrier atop the earth berm that is located on the windward side of the carriageways. This observation is counterintuitive, since the source is downwind to this structure for the prevailing wind. The CFD modeling indicates that such design can generated a large recirculation wake region formed on the leeward side of the wall that brings back to the wall the pollutant generated on the nearest traffic lanes. When the source is upwind of the wall noise barrier, i.e., wind in the opposite direction of the prevailing wind, this design hampers the pollutant dispersion contributing to enhance the PM deposition in front of the wall. This result is seldom described in the literature because studies are generally focused on the cases involving noise barriers downwind to the traffic in order to investigate their shielding impact off the motorway on residential areas.

The comparison between wall-top versus flat-top earth berms is only valid for the current state of the earth berms on which the vegetation is clear cut and not fully developed, because it was planted only two years before the survey. It seems important to reproduce this study when the vegetation will be woody and fully developed to check the impact of vegetated earth berms on the dispersion of

the near-traffic pollution. The question on the efficiency of vegetated earth berms to remove airborne pollutants by deposition is still pending to our knowledge and deserves to be explored. For this, it will be necessary to know a detailed quantification of deposition velocities and capture efficiencies for each endemic species installed on the earth berm in order to integrate in the CFD modeling a realistic dry deposition sink term. Since these parameters are not all available in the literature, a preliminary consistent study of wind tunnel experiments will be necessary.

5. Conclusions

We have evaluated the role of magnetic biomonitoring as further information to validate and strengthen CFD simulations of the dispersion of local traffic-related PM along a 12-lane motorway east to Montpellier, France. The test site comprises three flat-top earth berms and one roofed by a precast wall that were designed and installed by the motorway company to mitigate noise pollution. The innovative feature of this study is based on the multidisciplinary approach combining dustmeter measurements (e-PM μ-sensor), environmental magnetism, and XRF measurements as a constraint for a numerical model of fluid dynamics (CFD) based on the RANS equations (Reynolds-Averaged Navier–Stokes) and parameterized with the characteristics of the study area (highway development, prevailing wind direction, number of average circulating vehicles). The special feature of the CFD modeling is to consider the average road traffic by means of a volumetric source of average fleet turbulence, momentum, and PM emissions. All the data obtained in this study, whether experimental measurements or results from the CFD modeling, provide two clear conclusions:

- An asymmetry is evidenced in PM traffic-related depositions between the both sides of the motorway carriageways. A recirculation phenomenon and a blockage effect for the opposite wind direction is clearly observed around the noise barrier wall atop of the berm, while standard flat-top earth berms seem to favor the atmospheric dispersion of pollutants. The recent revegetation of merlons (only ≈50 cm high shrubs) clearly has no impact today on the mitigation effect of pollution.
- The IRM intensity of PM deposition on plant leaves has proven to be a useful and relevant tool well suited for an overview of near-source deposition of traffic-related PM with the relevant following precautions. The magnetic data have to be expressed by means of relative change to pinpoint the local traffic signal by subtracting the regional background of PM concentration. Storing the samples in a null-field environment for a few dozen minutes after the acquisition of IRM and before the measurements is required in order to avoid the viscous effect inherent to this type of magnetization.

Author Contributions: conceptualization, P.C. and S.L.; methodology, P.C., S.L., D.B.; analytical experiments, S.L., R.P., and P.C.; statistical analysis, S.L.; sampling, S.L., P.C., P.N., R.P.; Equipment maintenance, T.P. and P.N.; writing-original draft preparation, S.L. and P.C.; All authors have read and agreed to the published version of the manuscript.

Funding: This research was funded by the Agence Nationale de la Recherche (ANR) grant number ANR-19-CE04-0008 through the BREATHE project, and by a partnership agreement between the ASF/VINCI company and the CNRS, partnership number 169162, Air9 project.

Acknowledgments: We thank Mathilde Bardon, Cinderella Boyrie and Julie Faure for helping us during the soil sampling, as well as Julien Camps for his contribution in the development of the numerical topography and in the traffic simulations. We would particularly like to thank Georges Fandos from the MDPMA9 citizen association and the municipality of Saint-Aunès through its first magistrate, Alain Hugues, who have greatly contributed to the development of the experimental site along the motorway. We finally acknowledge the three anonymous reviewers for their constructive comments and discussion, which helped to improve the manuscript.

Conflicts of Interest: The authors declare no conflict of interest.

Appendix A

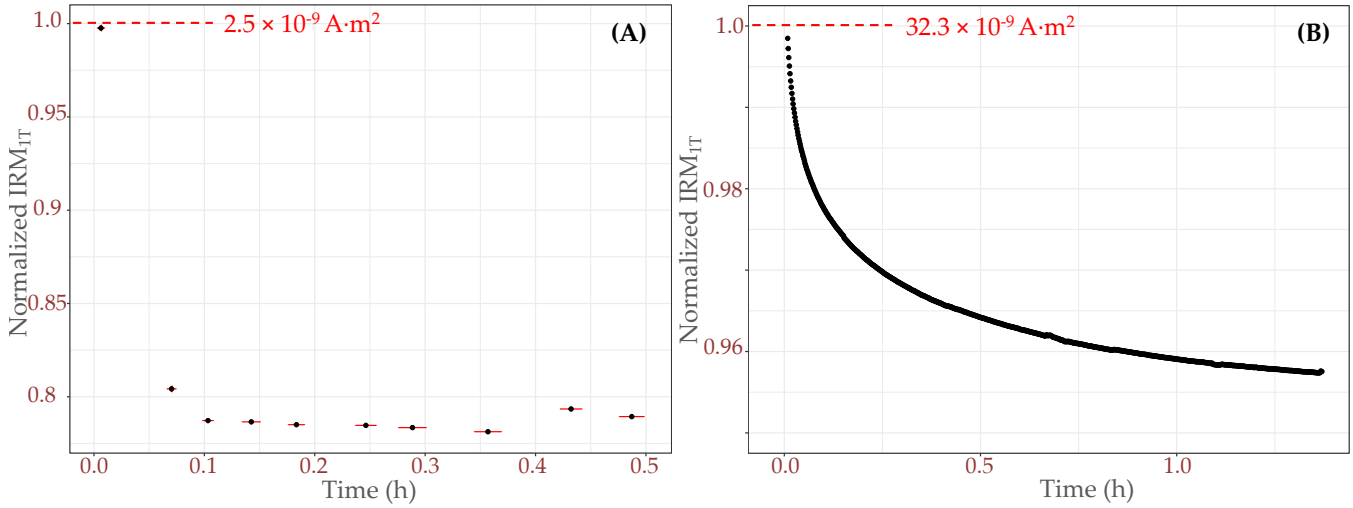

Figure A1. Normalized IRM_{1T} variations over the time for (**A**) sample holder and (**B**) holder filled with samples, illustrating the weak viscous effect due to the presence of iron-oxide impurities in the plastic molding such as superparamagnetic or a multi-domain like behavior particles.

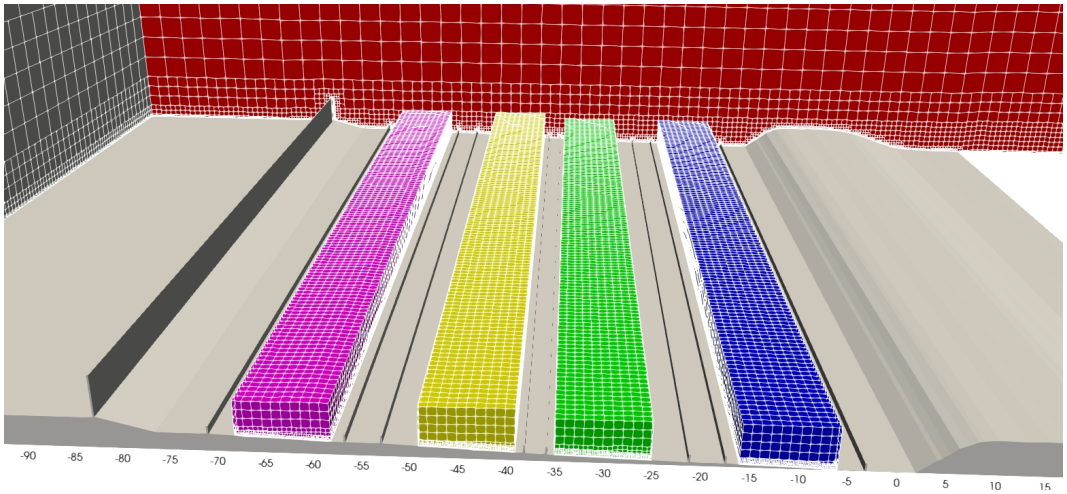

Figure A2. Four rectangular cuboids representing the traffic lanes and used as volumetric sources for the traffic momentum and turbulence in the modeling of the stationary wind velocity field and in the passive scalar equation as volumetric sources for PM emission.

References

1. Department of Economic and Social Affairs. *World Urbanization Prospects: The 2018 Revision*; UN: New York, NY, USA, 2019; ISBN 9789210043144.
2. Hama, S.M.L.; Cordell, R.L.; Monks, P.S. Quantifying primary and secondary source contributions to ultrafine particles in the UK urban background. *Atmos. Environ.* **2017**, *166*, 62–78, doi:10.1016/j.atmosenv.2017.07.013.
3. Kumar, P.; Morawska, L.; Birmili, W.; Paasonen, P.; Hu, M.; Kulmala, M.; Harrison, R.M.; Norford, L.; Britter, R. Ultrafine particles in cities. *Environ. Int.* **2014**, *66*, 1–10, doi:10.1016/j.envint.2014.01.013.
4. Stone, V.; Miller, M.R.; Clift, M.J.D.; Elder, A.; Mills, N.L.; Møller, P.; Schins, R.P.F.; Vogel, U.; Kreyling, W.G.; Alstrup Jensen, K.; et al. Nanomaterials Versus Ambient Ultrafine Particles: An Opportunity to Exchange Toxicology Knowledge. *Environ. Health Perspect.* **2017**, *125*, 106002, doi:10.1289/EHP424.
5. Newby, D.E.; Mannucci, P.M.; Tell, G.S.; Baccarelli, A.A.; Brook, R.D.; Donaldson, K.; Forastiere, F.; Franchini, M.; Franco, O.H.; Graham, I.; et al. Expert position paper on air pollution and cardiovascular disease. *Eur. Heart J.* **2015**, *36*, 83–93, doi:10.1093/eurheartj/ehu458.

6. Maher, B.A.; Ahmed, I.A.M.; Karloukovski, V.; MacLaren, D.A.; Foulds, P.G.; Allsop, D.; Mann, D.M.A.; Torres-Jardón, R.; Calderon-Garciduenas, L. Magnetite pollution nanoparticles in the human brain. *Proc. Natl. Acad. Sci. USA* **2016**, *113*, 10797–10801, doi:10.1073/pnas.1605941113.
7. European Environment Agency. *Air Quality in Europe—2019 Report*; EEA: Copenhagen, Denmark, 2019; Volume 10, Chapter 10; ISBN 978-92-9480-088-6.
8. Lelieveld, J.; Klingmüller, K.; Pozzer, A.; Pöschl, U.; Fnais, M.; Daiber, A.; Münzel, T. Cardiovascular disease burden from ambient air pollution in Europe reassessed using novel hazard ratio functions. *Eur. Heart J.* **2019**, *40*, 1590–1596, doi:10.1093/eurheartj/ehz135.
9. EUROPEAN COMMISSION. A Europe that protects: Clean air for all. Available online: https://ec.europa.eu/environment/air/pdf/clean_air_for_all.pdf (accessed on 5 June 2018).
10. Van Renterghem, T.; Botteldooren, D. On the choice between walls and berms for road traffic noise shielding including wind effects. *Landsc. Urban Plan.* **2012**, *105*, 199–210, doi:10.1016/j.landurbplan.2011.12.017.
11. Jeong, S.J. A CFD Study of Roadside Barrier Impact on the Dispersion of Road Air Pollution. *Asian J. Atmos. Environ.* **2015**, *9*, 22–30, doi:10.5572/ajae.2015.9.1.022.
12. Baldauf, R.; Thoma, E.; Khlystov, A.; Isakov, V.; Bowker, G.; Long, T.; Snow, R. Impacts of noise barriers on near-road air quality. *Atmos. Environ.* **2008**, *42*, 7502–7507, doi:10.1016/j.atmosenv.2008.05.051.
13. Hagler, G.S.W.; Lin, M.-Y.; Khlystov, A.; Baldauf, R.W.; Isakov, V.; Faircloth, J.; Jackson, L.E. Field investigation of roadside vegetative and structural barrier impact on near-road ultrafine particle concentrations under a variety of wind conditions. *Sci. Total Environ.* **2012**, *419*, 7–15, doi:10.1016/j.scitotenv.2011.12.002.
14. Mao, Y.; Wilson, J.D.; Kort, J. Effects of a shelterbelt on road dust dispersion. *Atmos. Environ.* **2013**, *79*, 590–598, doi:10.1016/j.atmosenv.2013.07.015.
15. Steffens, J.T.; Heist, D.K.; Perry, S.G.; Zhang, K.M. Modeling the effects of a solid barrier on pollutant dispersion under various atmospheric stability conditions. *Atmos. Environ.* **2013**, *69*, 76–85, doi:10.1016/j.atmosenv.2012.11.051.
16. Tong, Z.; Baldauf, R.W.; Isakov, V.; Deshmukh, P.; Max Zhang, K. Roadside vegetation barrier designs to mitigate near-road air pollution impacts. *Sci. Total Environ.* **2016**, *541*, 920–927, doi:10.1016/j.scitotenv.2015.09.067.
17. Ozdemir, H. Mitigation impact of roadside trees on fine particle pollution. *Sci. Total Environ.* **2019**, *659*, 1176–1185, doi:10.1016/j.scitotenv.2018.12.262.
18. Ram, S.S.; Majumder, S.; Chaudhuri, P.; Chanda, S.; Santra, S.C.; Chakraborty, A.; Sudarshan, M. A Review on Air Pollution Monitoring and Management Using Plants With Special Reference to Foliar Dust Adsorption and Physiological Stress Responses. *Crit. Rev. Environ. Sci. Technol.* **2015**, *45*, 2489–2522, doi:10.1080/10643389.2015.1046775.
19. Janhäll, S. Review on urban vegetation and particle air pollution—Deposition and dispersion. *Atmos. Environ.* **2015**, *105*, 130–137, doi:10.1016/j.atmosenv.2015.01.052.
20. Abhijith, K.V.; Kumar, P. Quantifying particulate matter reduction and their deposition on the leaves of green infrastructure. *Environ. Pollut.* **2020**, *265*, 114884, doi:10.1016/j.envpol.2020.114884.
21. Hofman, J.; Maher, B.A.; Muxworthy, A.R.; Wuyts, K.; Castanheiro, A.; Samson, R. Biomagnetic Monitoring of Atmospheric Pollution: A Review of Magnetic Signatures from Biological Sensors. *Environ. Sci. Technol.* **2017**, *51*, 6648–6664, doi:10.1021/acs.est.7b00832.
22. Maher, B.A.; Moore, C.; Matzka, J. Spatial variation in vehicle-derived metal pollution identified by magnetic and elemental analysis of roadside tree leaves. *Atmos. Environ.* **2008**, *42*, 364–373, doi:10.1016/j.atmosenv.2007.09.013.
23. Castanheiro, A.; Samson, R.; De Wael, K. Magnetic- and particle-based techniques to investigate metal deposition on urban green. *Sci. Total Environ.* **2016**, *571*, 594–602, doi:10.1016/j.scitotenv.2016.07.026.
24. Wang, H.; Maher, B.A.; Ahmed, I.A.M.; Davison, B. Efficient Removal of Ultrafine Particles from Diesel Exhaust by Selected Tree Species: Implications for Roadside Planting for Improving the Quality of Urban Air. *Environ. Sci. Technol.* **2019**, *53*, 6906–6916, doi:10.1021/acs.est.8b06629.
25. Maher, B.A.; Thompson, R. *Quaternary Climates, Environments and Magnetism*; Maher, B.A., Thompson, R., Eds.; Cambridge University Press: Cambridge, UK, 1999; ISBN 9780521624176.

26. Dzierżanowski, K.; Popek, R.; Gawrońska, H.; Sæbø, A.; Gawroński, S.W. Deposition of Particulate Matter of Different Size Fractions on Leaf Surfaces and in Waxes of Urban Forest Species. *Int. J. Phytoremediation* **2011**, *13*, 1037–1046, doi:10.1080/15226514.2011.552929.
27. Przybysz, A.; Sæbø, A.; Hanslin, H.M.; Gawroński, S.W. Accumulation of particulate matter and trace elements on vegetation as affected by pollution level, rainfall and the passage of time. *Sci. Total Environ.* **2014**, *481*, 360–369, doi:10.1016/j.scitotenv.2014.02.072.
28. Chiam, Z.; Song, X.P.; Lai, H.R.; Tan, H.T.W. Particulate matter mitigation via plants: Understanding complex relationships with leaf traits. *Sci. Total Environ.* **2019**, *688*, 398–408, doi:10.1016/j.scitotenv.2019.06.263.
29. Castanheiro, A.; Hofman, J.; Nuyts, G.; Joosen, S.; Spassov, S.; Blust, R.; Lenaerts, S.; De Wael, K.; Samson, R. Leaf accumulation of atmospheric dust: Biomagnetic, morphological and elemental evaluation using SEM, ED-XRF and HR-ICP-MS. *Atmos. Environ.* **2020**, *221*, 117082, doi:10.1016/j.atmosenv.2019.117082.
30. Cao, L.; Appel, E.; Hu, S.; Ma, M. An economic passive sampling method to detect particulate pollutants using magnetic measurements. *Environ. Pollut.* **2015**, *205*, 97–102, doi:10.1016/j.envpol.2015.05.019.
31. Néel, L. Théorie du traînage magnétique des ferromagnétiques en grains fins avec application aux terres cuites. *Ann. Géophys.* **1949**, *5*, 99–136.
32. Sagnotti, L.; Taddeucci, J.; Winkler, A.; Cavallo, A. Compositional, morphological, and hysteresis characterization of magnetic airborne particulate matter in Rome, Italy. *Geochem. Geophys. Geosyst.* **2009**, *10*, doi:10.1029/2009GC002563.
33. Guo, L.; Maghirang, R.G. Numerical Simulation of Airflow and Particle Collection by Vegetative Barriers. *Eng. Appl. Comput. Fluid Mech.* **2012**, *6*, 110–122, doi:10.1080/19942060.2012.11015407.
34. Bonifacio, H.F.; Maghirang, R.G.; Glasgow, L.A. Numerical Simulation of Transport of Particles Emitted From Ground-Level Area Source Using Aermod and CFD. *Eng. Appl. Comput. Fluid Mech.* **2014**, *8*, 488–502, doi:10.1080/19942060.2014.11083302.
35. Jeanjean, A.P.R.; Hinchliffe, G.; McMullan, W.A.; Monks, P.S.; Leigh, R.J. A CFD study on the effectiveness of trees to disperse road traffic emissions at a city scale. *Atmos. Environ.* **2015**, *120*, 1–14, doi:10.1016/j.atmosenv.2015.08.003.
36. ACEA. Vehicles in Use Europe 2019. Available online: https://www.acea.be/publications/article/report-vehicles-in-use-europe-2019 (accessed on 15 July 2020).
37. Wang, X.; Khlystov, A.; Ho, K.-F.; Campbell, D.; Chow, J.C.; Kohl, S.D.; Watson, J.G.; Lee, S.-C.F.; Chen, L.-W.A.; Lu, M.; et al. Real-World Vehicle Emissions Characterization for the Shing Mun Tunnel in Hong Kong and Fort McHenry Tunnel in the United States. *Res. Rep. Health. Eff. Inst.* 2019. Available online: https://www.ncbi.nlm.nih.gov/pmc/articles/PMC7282032/ (accessed on 25 November 2020).
38. Lawrence, S.; Sokhi, R.; Ravindra, K. Quantification of vehicle fleet PM10 particulate matter emission factors from exhaust and non-exhaust sources using tunnel measurement techniques. *Environ. Pollut.* **2016**, doi:10.1016/j.envpol.2016.01.011.
39. Abu-Allaban, M.; Coulomb, W.; Gertler, A.W.; Gillies, J.; Pierson, W.R.; Rogers, C.F.; Sagebiel, J.C.; Tarnay, L. Exhaust Particle Size Distribution Measurements at the Tuscarora Mountain Tunnel. *Aerosol Sci. Technol.* **2002**, *36*, 771–789, doi:10.1080/02786820290038401.
40. Blocken, B. Computational Fluid Dynamics for urban physics: Importance, scales, possibilities, limitations and ten tips and tricks towards accurate and reliable simulations. *Build. Environ.* **2015**, *91*, 219–245, doi:10.1016/j.buildenv.2015.02.015.
41. Jones, W..; Launder, B.. The prediction of laminarization with a two-equation model of turbulence. *Int. J. Heat Mass Transf.* **1972**, *15*, 301–314, doi:10.1016/0017-9310(72)90076-2.
42. Peralta, C.; Nugusse, H.; Kokilavani, S.P.; Schmidt, J.; Stoevesandt, B. Validation of the simpleFoam (RANS) solver for the atmospheric boundary layer in complex terrain. *ITM Web Conf.* **2014**, *2*, 01002, doi:10.1051/itmconf/20140201002.
43. Solazzo, E.; Cai, X.; Vardoulakis, S. Modelling wind flow and vehicle-induced turbulence in urban streets. *Atmos. Environ.* **2008**, *42*, 4918–4931, doi:10.1016/j.atmosenv.2008.02.032.
44. Wang, Y.J.; Nguyen, M.T.; Steffens, J.T.; Tong, Z.; Wang, Y.; Hopke, P.K.; Zhang, K.M. Modeling multi-scale aerosol dynamics and micro-environmental air quality near a large highway intersection using the CTAG model. *Sci. Total Environ.* **2013**, *443*, 375–386, doi:10.1016/j.scitotenv.2012.10.102.

45. Buccolieri, R.; Jeanjean, A.P.R.; Gatto, E.; Leigh, R.J. The impact of trees on street ventilation, NOx and PM2.5 concentrations across heights in Marylebone Rd street canyon, central London. *Sustain. Cities Soc.* **2018**, *41*, 227–241, doi:10.1016/j.scs.2018.05.030.
46. Bowker, G.E.; Baldauf, R.; Isakov, V.; Khlystov, A.; Petersen, W. The effects of roadside structures on the transport and dispersion of ultrafine particles from highways. *Atmos. Environ.* **2007**, *41*, 8128–8139, doi:10.1016/j.atmosenv.2007.06.064.
47. Reiminger, N.; Jurado, X.; Vazquez, J.; Wemmert, C.; Blond, N.; Dufresne, M.; Wertel, J. Effects of wind speed and atmospheric stability on the air pollution reduction rate induced by noise barriers. *J. Wind Eng. Ind. Aerodyn.* **2020**, *200*, 104160, doi:10.1016/j.jweia.2020.104160.
48. Patterson, R.F.; Harley, R.A. Evaluating near-roadway concentrations of diesel-related air pollution using RLINE. *Atmos. Environ.* **2019**, *199*, 244–251, doi:10.1016/j.atmosenv.2018.11.016.
49. Franke, J.; Hellsten, A.; Schlünzen, H.; Carissimo, B. *Best Practice Guideline for the CFD Simulation of Flows in the Urban Environment*; European Cooperation in Science and Technology: Brussels, Belgium, 2007; ISBN 3000183124.
50. Richards, P.J.; Norris, S.E. Appropriate boundary conditions for computational wind engineering models revisited. *J. Wind Eng. Ind. Aerodyn.* **2011**, *99*, 257–266, doi:10.1016/j.jweia.2010.12.008.
51. Richards, P.J.; Norris, S.E. Appropriate boundary conditions for computational wind engineering: Still an issue after 25 years. *J. Wind Eng. Ind. Aerodyn.* **2019**, *190*, 245–255, doi:10.1016/j.jweia.2019.05.012.
52. Van Doormaal, J.P.; Raithby, G.D. Enhancements of the Simple Method for Predicting Incompressible Fluid Flows. *Numer. Heat Transf. Part B Fundam.* **1984**, *7*, 147–163, doi:10.1080/10407798408546946.
53. Lê, S.; Josse, J.; Husson, F. FactoMineR : An R Package for Multivariate Analysis. *J. Stat. Softw.* **2008**, *25*, doi:10.18637/jss.v025.i01.
54. De Miguel, E.; Llamas, J.F.; Chacón, E.; Berg, T.; Larssen, S.; Røyset, O.; Vadset, M. Origin and patterns of distribution of trace elements in street dust: Unleaded petrol and urban lead. *Atmos. Environ.* **1997**, *31*, 2733–2740, doi:10.1016/S1352-2310(97)00101-5.
55. Sternbeck, J.; Sjödin, Å.; Andréasson, K. Metal emissions from road traffic and the influence of resuspension—results from two tunnel studies. *Atmos. Environ.* **2002**, *36*, 4735–4744, doi:10.1016/S1352-2310(02)00561-7.
56. Carsignol, J.; Calovi, L. *La Pollution des Sols et des Végétaux à Proximité des Routes—Les éléments Traces Métalliques (ETM)*; SETRA: Sourdun, France, 2004.
57. Birmili, W.; Allen, A.G.; Bary, F.; Harrison, R.M. Trace metal concentrations and water solubility in size-fractionated atmospheric particles and influence of road traffic. *Environ. Sci. Technol.* **2006**, *40*, 1144–1153, doi:10.1021/es0486925.
58. Weckwerth, G. Verification of traffic emitted aerosol components in the ambient air of Cologne (Germany). *Atmos. Environ.* **2001**, *35*, 5525–5536, doi:10.1016/S1352-2310(01)00234-5.
59. Sarkar, B. *Heavy Metals in the Environment*; CRC Press: Boca Raton, FL, USA, 2002; ISBN 0203909305, 9780203909300.
60. Veschambre, S. Caractérisation et Quantification des Eléments Traces Métalliques Dans les Dépôts et les Particules Atmosphériques de la Vallée d'Aspe-Mise en Place d'Indicateurs de la Qualité de l'Air, Ph.D. Thesis, Ecole Doctorale des Sciences Exactes et de leurs Applications, Universite de Pau et de Pays de l'Adour, Pau, France, 2006.
61. Pant, P.; Harrison, R.M. Estimation of the contribution of road traffic emissions to particulate matter concentrations from field measurements: A review. *Atmos. Environ.* **2013**, *77*, 78–97, doi:10.1016/j.atmosenv.2013.04.028.
62. Zenodo open-access repository. Available online: https://zenodo.org/record/3961496#.X7vOTqpKiwU (accessed on 8th August 2020).
63. ICCT. DielselNet Transport Policy. Available online: https://www.transportpolicy.net (accessed on 15 June 2020).
64. Lin, Y.-C.; Tsai, C.-J.; Wu, Y.-C.; Zhang, R.; Chi, K.-H.; Huang, Y.-T.; Lin, S.-H.; Hsu, S.-C. Characteristics of trace metals in traffic-derived particles in Hsuehshan Tunnel, Taiwan: Size distribution, potential source, and fingerprinting metal ratio. *Atmos. Chem. Phys.* **2015**, *15*, 4117–4130, doi:10.5194/acp-15-4117-2015.